RSC Advances

PAPER

View Article Online
View Journal | View Issue

Cite this: *RSC Adv.*, 2014, **4**, 24272

Multi-functional ceramic hybrid coatings on biodegradable AZ31 Mg implants: electrochemical, tribological and quantum chemical aspects for orthopaedic applications†

A. Madhankumar,*[a] Elangovan Thangavel,[b] Suresh Ramakrishna,[c] I. B. Obot,[a] Hwa Chul Jung,[d] Kwang Seon Shin,[d] Zuhair M. Gasem,[a] Hyongbum Kim[c] and Dae-Eun Kim*[be]

Received 18th March 2014
Accepted 6th May 2014

DOI: 10.1039/c4ra02363c

www.rsc.org/advances

Application of biodegradable implants has received increasing attention for the treatment of bone damage due to their low adverse effects. To achieve better biocompatibility and enhanced corrosion resistance of biodegradable implants with improved wear resistance, multifunctional coatings need to be developed. Herein, a ceramic hybrid coating has been fabricated by a plasma electrolytic oxidation (PEO) technique using Ta_2O_5 nanoparticle inclusion on AZ31 Mg alloy in order to attain superior corrosion, wear behavior, and surface porosity that enable improved bioactivity. X-ray diffraction analysis of PEO coatings showed that the surface coating is mainly composed of $Mg_3(PO_4)_2$, MgO and Ta_2O_5 in different quantities based on PEO processing. Furthermore, scanning electron microscopy (SEM) analysis was employed to observe the surface of the resultant PEO hybrid coatings after and before wear tests. With Ta_2O_5 nanoparticles, PEO coatings showed excellent wear compared with pure PEO coatings. The efficiency of the hybrid coatings in corrosion protection was verified by the Tafel plot and electrochemical impedance spectroscopy measurements in simulated body fluid. Furthermore, *in vitro* cell culture studies were performed on MG-63 human cells to evaluate the biocompatibility of PEO coatings. A quantum chemical approach and force-field molecular dynamics simulation were employed to evaluate the interaction between the AZ31 Mg surface and PEO hybrid coatings. All of the observations evidently showed that the ceramic hybrid PEO coating provides improved wear and corrosion protection performance with superior biocompatibility with Ta_2O_5 nanoparticles, when compared to pure PEO coatings, due to its synergistic beneficial effect.

1. Introduction

In recent years, considerable research efforts have been devoted to design advanced implant materials of light weight and superior mechanical strength due to the urgent need for their use in a variety of biomedical applications. Magnesium (Mg) and its alloys, in particular, have been extensively studied because of their unique properties such as low density, high specific strength and stiffness, excellent castability and machinability. Moreover, Mg-based alloys have a natural ability to biodegrade when placed in aqueous solutions, which is promising for short-term or temporary implants in orthopaedic applications. However, because of certain limitations, they are not adequate for use as orthopaedic implants; hence, proper surface treatment is required to enhance their performance. Up to now, various strategies, including physical vapor deposition (PVD), thermal spraying and hard anodizing, have been designed to overcome these shortcomings.[1–3] Nevertheless, most of the methods mentioned above involve high temperature during processing, which inevitably degrade the coating and substrate; hence, they are not suitable for the deposition of surface coatings on biodegradable Mg implants.

Plasma electrolytic oxidation (PEO), a new surface modification technique based on anodic oxidation, has been adopted for surface treatment of Mg alloys in recent years to improve their corrosion resistance and tribological performance.[4–6] With

[a]*Center of Research Excellence in Corrosion, Research Institute, King Fahd University of Petroleum and Minerals, Dhahran-31261, Kingdom of Saudi Arabia. E-mail: madhankumar@kfupm.edu.sa; Fax: +966538604818; Tel: +966538801789*

[b]*Center for Nano-Wear, Yonsei University, Seoul 120-749, Republic of Korea*

[c]*Graduate School of Biomedical Science and Engineering/College of Medicine, Hanyang University, Sungdong-gu, Seoul, South Korea*

[d]*Magnesium Technology Innovation Center, School of Materials Science and Engineering, Seoul National University, Seoul 151-744, Republic of Korea*

[e]*Department of Mechanical Engineering, Yonsei University, Seoul 120-749, Republic of Korea. E-mail: kimde@yonsei.ac.kr*

† Electronic supplementary information (ESI) available. See DOI: 10.1039/c4ra02363c

PEO, the composition and structure of coatings can be tailored readily by controlling the electrolyte composition and concentration. To date, conventional PEO coatings on Mg alloys are employed in electrolytes containing sodium silicate, phosphate and aluminate,[7] and the resultant coatings are generally composed of amorphous and/or crystalline phases like MgO, Mg_2SiO_4 and $Mg_3(PO_4)_2$. However, the stability of MgO in acid or neutral solution is low, which further restricts the corrosion resistance and biological performance of coatings. Apparently, the optimum way to produce PEO coatings with multi-functional performance on Mg alloys is to reduce the defects and increase the content of chemically stable compounds by developing novel electrolyte systems. In recent years, most research has focused on improving the corrosion behavior and biocompatibility of PEO coatings containing more stable oxides and compounds, such as TiO_2, ZrO_2, CeO_2, $Mg_2Zr_5O_{12}$, Al_2O_3 and silica, by varying the constituents of the electrolytes.[8–10]

Tantalum (Ta) and Ta-based compounds are considered as promising materials for biomedical applications, since they exhibit high fracture toughness, corrosion and wear resistance, and chemical stability.[11] Donkov *et al.* verified the *in vitro* cytocompatibility of Ta_2O_5 coatings, and their results demonstrated good cytocompatibility of the Ta_2O_5 coatings with optimum stoichiometric Ta_2O_5 composition.[12] However, biocompatibility and corrosion with tribological characteristics of PEO coatings formed on Mg alloys are seldom studied. Hence, a biodegradable Mg alloy with better surface biocompatibility and enhanced wear and corrosion resistances is essential for wider clinical acceptance. To explore the potential benefits of tantalum oxide (Ta_2O_5) nanoparticles in PEO coatings on Mg alloys, this present study investigated the corrosion as well as tribological performance of PEO coatings deposited on an AZ31 Mg alloy in electrolytes with different Ta_2O_5 nanoparticle concentrations. *In vitro* cell culture studies were conducted on MG-63 human cells to check the biocompatibility of coated AZ31 Mg substrates. A quantum chemical calculation complemented with molecular dynamics simulations was further applied to provide some insights into the stability of the coating film.

2. Experimental procedure

2.1. Preparation of substrates

The substrate material used for the present investigation was strip-cast AZ31 magnesium alloy with a chemical composition (wt%) of 2.5–3.5 Al, 0.6–1.5 Zn, 0.2 Mn, 0.1 Si, 0.05 Cu, 0.001 Ni, 0.001 Fe, and balance Mg. The substrates with a size of 20 mm × 50 mm × 3.35 mm were cut and ground with different grit size of SiC papers ranging from 400 to 2400.

2.2. Preparation of PEO ceramic coatings

The PEO treatment was performed with a pulsed DC electrical power source with the AZ31 Mg alloy substrate and a stainless steel cylinder container acting as anode and cathode, respectively. The electrolytic solution was composed of an aqueous solution of KOH (0.03 M), KF (0.05 M) and Na_3PO_4 (0.2 M) without and with Ta_2O_5 nanoparticles (1, 5 and 10 mg L^{-1}), respectively. The temperature of the electrolytes during the treatment was constantly maintained at 20 ± 2 °C by a water cooling system, and the electrolyte was stirred continuously during the treatment. The PEO coating was prepared in this solution at a current density of 7 mA cm^{-2} for an oxidation time of 1200 s. The pulse frequency and duty ratio employed were 500 Hz and 50%, respectively. The processed PEO coatings without and with 1, 5, and 10 mg L^{-1} Ta_2O_5 nanoparticles are referred to as pure PEO, Ta1, Ta5, and Ta10, respectively.

2.3. Surface characterization of PEO coatings

PEO-coated substrates were observed in the plane view and in cross-sectional view by SEM, using a JSM-6360 (JEOL) instrument operated at 20 kV coupled with energy-dispersive X-ray (EDAX) analysis. The phase composition of PEO coatings was studied by X-ray diffraction (XRD) by Cu and Co Kα radiation using Philips X'Pert-MPD (PW 3040) with a step size 0.005° and a scan range from 10° to 80° (in 2θ).

In order to evaluate the mechanical performance of the coated AZ31 Mg substrates, a microhardness test was also carried out using The Ever one, Model no. MH-3 microhardness tester. Hardness measurements were performed on the surfaces at a load of 250 mN and dwell time of 12 s. Vickers hardness (HV) value was calculated by dividing the indentation force by the surface of the imprint observed under the microscope. For each substrate, at least 10 measurements were made at various sites.

Contact angles were measured using a sessile drop method with a Kruss G10 contact angle apparatus. A drop of SBF (5 μl) was positioned on the coated substrates and photographed immediately after positioning. The images of drops were processed by the image analysis system, which calculated contact angles from the shapes of the drops with an accuracy of ±0.1°. Note that the uncoated AZ31 Mg substrate was considered as control, and to achieve an accurate value, ten measurements were collected for each substrate.

2.4. Tribological studies

The friction and wear properties of the PEO coating were studied using a commercial reciprocating tribo-tester. An Al_2O_3 sphere with a diameter of 1 mm was employed as the counter surface after a standard cleaning procedure. All measurements were performed under the following conditions: room temperature, relative humidity of about 40%, applied load of 50 mN, and sliding speed of 2 mm s^{-1} with a 4 mm stroke. The friction coefficient (CoF) and number of sliding cycles were registered automatically through a data acquisition system. In order to get an average friction value, the experiments were repeated five times for each specimen. The standard wear equation proposed by Archard was used to obtain the wear rate:

$$\text{Wear rate} = V/W \times L \quad (1)$$

where V is the wear volume, W is the applied load, and L is the sliding distance.

2.5. Electrochemical characterization of PEO coatings

In order to evaluate the corrosion performance of the PEO coatings both polarization and EIS tests were performed in SBF solution using coated substrates for each of these tests. Prior to the measurements, the substrates were immersed in the test solution for 30 min to reach a stable open circuit potential (OCP). The standard three-electrode cell assembly consisted of a saturated calomel electrode (SCE) as a reference electrode, a Pt sheet as a counter electrode and the coated substrates as the working electrode. Polarization curves for uncoated and coated substrates were recorded under potentiodynamic conditions in the potential range ±250 mV with respect to OCP at a sweep rate of 1 mV s^{-1}. The EIS equipment was set up in the frequency range between 0.01 and 10^4 Hz with amplitude of ±10 mV. The analysis of the impedance spectra and fitting of the experimental results to equivalent circuits was performed using ZSimpWin 3.21, which allowed the chi-square (χ^2) value to ascertain the quality of the equivalent circuit fitting. In order to test the reproducibility of the results, the experiments were performed in triplicate.

2.6. Cell culture studies

MG-63 cells, a human osteosarcoma cell line, were purchased from Korean Cell Line Bank and cultured in 5% CO_2 at 37 °C in cell incubators using DMEM (GIBCO-BRL, Rockville, MD) supplemented with 10% FBS and 1% penicillin and streptomycin.

2.7. Live viability assay

For a live cell viability assay, AZ31 Mg substrates coated with different concentrations of Ta_2O_5 were placed on 6-well dishes and sterilized under ultraviolet radiation for 1 h. MG-63 cells (1×10^5) were seeded on the sterile samples, and the plates containing samples were incubated in a cell incubator. The assay was performed on days 3 and 7 using LIVE/DEAD Viability/Cytotoxicity Kit (Molecular Probes, USA). Cells were washed gently three time using 1× PBS. Fluorescent dyes containing calcein AM at a working concentration of 2 μM in PBS were used to stain the cells, and the plates were incubated for 20 min. in the dark at room temperature. The images of living cells, which appeared green in colour, were captured using fluorescence microscopy.

2.8. Cell counting assay

Equal numbers of MG-63 cell suspensions (1×10^5 cells) were seeded on 6-well plates each containing AZ31 Mg substrates coated with different concentrations of Ta_2O_5. The cells were allowed to grow on the specimens for 3 and 7 days. Specimens were transferred to new 6-well plates and the assay was performed as per the protocol provided by Cell Counting Kit-8 (CCK-8) kit (Dojindo, Molecular Technologies, Rockville, MD, USA). Absorbance was measured at 450 nm using a spectrophotometer.

3. Results and discussion

3.1. Voltage–time curve

Fig. 1 depicts the variation of the anodic voltage as a function of treatment time during the PEO process in the electrolyte with and without Ta_2O_5 nanoparticles. The voltage variations may probably be categorized into three regions based on increasing rate. In the first region, the voltage was rapidly increased for about 10 s and this rapid increase of voltage appears to be due to the formation of a passive film on the AZ31 Mg alloy. In the second region, the rate of increase in voltage is lower than that in the first region. During this stage, breakdown of the passive film occurred as a result of the increased voltage, and small sparks and microarcs were seen. In the third region, *i.e.*, from approximately 150 s, the voltage was slightly increased and larger sized arcs appeared. The voltage response behavior according to the time was similar for electrolyte with and without Ta_2O_5 nanoparticles. However, the voltage response of electrolyte with Ta_2O_5 nanoparticles in the second and third regions was significantly higher than that for electrolyte without Ta_2O_5 nanoparticles.

In order to obtain clear information about the growth rate of PEO coatings with Ta_2O_5 nanoparticles, the weight gain of ceramic coatings was measured and the plot obtained is shown in Fig. S1 (ESI†). As can be seen from the figure, it is clear that PEO coatings with Ta_2O_5 nanoparticles showed higher weight gain than pure PEO coatings. In addition, we have also measured the coating thickness and conductivity of electrolyte, and the values obtained are displayed in Table 1. As shown in Table 1, it is clear that the average coating thickness increases linearly with the addition of Ta_2O_5 in the electrolyte. The distinct deviation in the above obtained behavior is ascribed to the variance in the conductivity of the electrolytes with and without Ta_2O_5 nanoparticles. It can be seen that the conductivity of phosphate electrolyte with Ta_2O_5 nanoparticles (10.8 mS cm^{-1}) is lower than the conductivity of phosphate electrolyte without Ta_2O_5 nanoparticles (28.5 mS cm^{-1}). In the case of

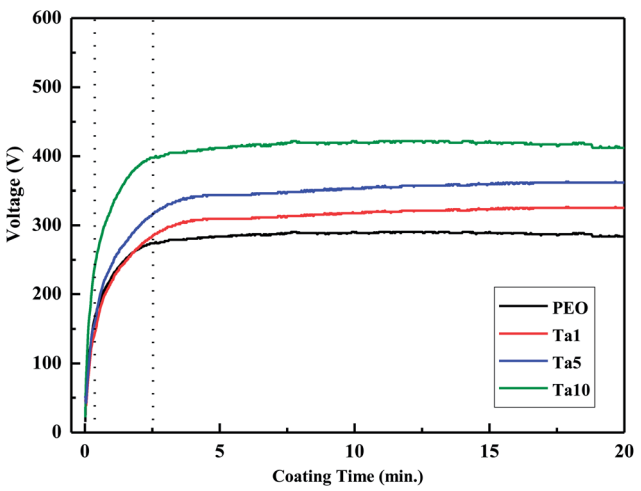

Fig. 1 Voltage-time response curves during PEO processing for different amounts of Ta_2O_5 nanoparticles on AZ31 Mg substrate.

Table 1 Description of PEO coatings on AZ31 Mg substrates

S. no.	Description	Conductivity of electrolytes (mS cm^{-1})	Final voltage (V)	Thickness (±0.1 μm)	Adhesion remaining (%)
1	Pure PEO	28.5	286	12.5	95
2	Ta1	22.4	325	13.8	95
3	Ta5	18.6	361	14.6	95
4	Ta10	10.8	413	15.7	95

PEO coatings with Ta_2O_5 nanoparticles, breakdown voltage increases due to low conductivity of Ta_2O_5 nanoparticles in the electrolyte, thereby increasing the growth rate of PEO coating.[13] Moreover, the different breakdown voltages indicated that the plasma chemical reactions at the substrate/electrolyte interface were relatively different. Hence, it is more valuable to investigate the anti-corrosion and wear characteristics of PEO coatings processed in the electrolytes with and without Ta_2O_5 nanoparticles.

3.2. XRD analysis

Fig. 2 shows the XRD patterns of pure PEO and PEO hybrid coatings on AZ31 Mg substrates. It can be seen that the PEO coatings were mainly composed of $Mg_3(PO_4)_2$, MgO and Ta_2O_5 nanoparticles depending on mode of processing. Note that the intensity of peaks corresponding to the $Mg_3(PO_4)_2$ and MgO became stronger and the substrate peaks were not observed, which clearly showed that X-ray intensity was not enough to reach the alloy substrate due to the formation of thicker and compact coatings. The appearance of peaks at 22.5°, 26.6°, 36.3° and 56.5° are attributed to Ta_2O_5 nanoparticles in PEO coatings (JCPDS: 19-1299). The X-ray diffractogram showed Ta_2O_5 nanoparticles to be crystalline in nature and have a hexagonal phase with the crystallite size in the range of 50–60 nm. In addition, the intensity of tantalum oxide peaks increased with increasing concentration of Ta_2O_5 nanoparticles in the electrolyte, which further confirms the appearance of Ta_2O_5 nanoparticles in the PEO coatings. Guo *et al.* reported that the rate of film formation increased when the elements with higher conductivity were introduced to the coating solution,[14] which is in good agreement with the observed results. Furthermore, the relative content of detected phases in the coatings is measured based on the intensities of diffraction peaks and is shown in Fig. S2 (ESI†). The relative content of MgO in PEO coatings is smaller than that of others, which clearly revealed that the MgO exists as a thin barrier layer and the outer layer mainly consists of $Mg_3(PO_4)_2$ and Ta_2O_5 in different quantities.

3.3. SEM results

Typical porous morphology induced by the intensive sparking during the PEO process can be seen in Fig. 3a–d. In the case of pure PEO coatings, relatively lower-sized micropores were observed without cracks on the entire coating surface, whereas PEO coatings with nanoparticles showed evenly distributed pores that have mainly irregular shapes and different sizes. Interestingly, many Ta_2O_5 nanoparticles with sizes of ~50 nm could be found on the surface of the substrates processed in the electrolyte with Ta_2O_5 nanoparticles (Fig. 3b). It has been reported that the incorporation of nanoparticles during PEO of Mg alloys could result in the combined effects of electrophoretic interaction and mechanical intermixing of attracted nanoparticles close to the anodic electrode with fluctuating molten magnesium oxide.[15] To further confirm the presence of Ta_2O_5 nanoparticles on PEO coatings, SEM with EDAX mapping analysis was carried out and the obtained results are given in Fig. S3 (ESI†). EDAX mapping images clearly confirmed the presence of Ta_2O_5 nanoparticles on PEO coatings, which strongly supports the incorporation of Ta_2O_5 nanoparticles. The

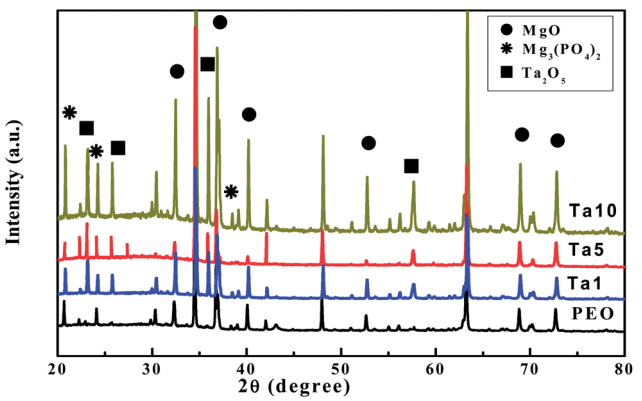

Fig. 2 XRD patterns of PEO coated AZ31 substrates with and without Ta_2O_5 nanoparticles.

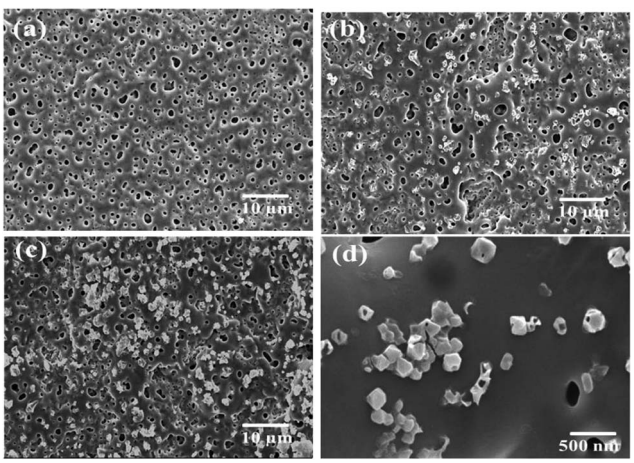

Fig. 3 SEM images of (a) PEO (b) Ta1 (c) Ta5 and (d) Ta10 (high magnification) coatings on AZ31 Mg substrates.

differences in the surface morphology of PEO coatings with and without Ta_2O_5 nanoparticles have been described in the present study. In general, the different surface morphologies of the PEO coatings may be ascribed to the different discharge characteristics during the PEO process. The pores were formed on the coating surface when the molten oxide and gas bubbles were released through the discharge channels. Furthermore, the lower Pilling–Bedworth ratio (PBR) of magnesia (PBR of a metal oxide is defined as the ratio of the volume of the metal oxide to the consumed metal volume) is also a significant reason for high porosity of PEO films on magnesium alloys. Few microcracks on the coating surface of PEO with Ta_2O_5 could also be formed by excessive thermal stress from the rapid solidification of Ta_2O_5 melted in the discharge tunnel by the electrolyte acting as coolant; hence, the appearance of cracks is inevitable. Therefore, the number and sizes of pores depend on the number and sizes of sparks at the end of the PEO process. In other words, the pore characteristics depend on the final voltages, as high final voltage results in large sparks on coating surface.[16] In the presence of phosphate electrolyte without Ta_2O_5 nanoparticles, the sparks were small, abundant, and evenly distributed; however, the sparks in the presence of phosphate electrolytes with Ta_2O_5 were larger, as their final voltages were larger (Table 1). Furthermore, the sparks in the electrolyte with 1 mg L^{-1} Ta_2O_5 were relatively even. It was observed that increasing the addition of Ta_2O_5 nanoparticles in the electrolytes resulted in more intensive discharging sparks at the sample surface during the PEO process, which led to development of cracks and bumps that caused the coating becoming rough and uneven. In particular, electrolyte with 10 mg L^{-1} Ta_2O_5 had several large and prolonged sparks scattered among a large number of small sparks, which makes it show higher surface roughness with different surface morphology among the coated substrates.

Fig. 4a and b shows the cross-sectional micrographs of the PEO coatings obtained on AZ31 Mg substrates with and without Ta_2O_5 nanoparticles. It is observed from the figures that PEO coatings are composed of an outer porous layer and an inner barrier layer. Furthermore, cracks did not appear in the cross-sectional images, which indicates a strong adhesion of the coating to Mg substrate. In addition, the color distribution of the cross-sectional PEO coating is not uniform, which demonstrated that the distribution of the elements in the coating is inhomogeneous. Thickness of the coatings formed in electrolyte with nanoparticles is higher compared with the coatings processed by electrolyte without nanoparticles. This indicates that the growth rates of coatings formed in the electrolytes with nanoparticles are relatively high and the addition of Ta_2O_5 nanoparticles enhances the growth of the coating during the PEO process.

3.4. Microhardness results

Fig. 5 shows the microhardness values of uncoated and PEO coated AZ31 Mg substrates. Statistical analysis was conducted to evaluate significant differences in hardness values among coated substrates and the results of the statistical analysis are shown in Table S5 (ESI†). The average hardness value of PEO coated AZ31 Mg substrates exhibited significant scattering due to the fact that micropores exist on the coating surface.[17] However, the average microhardness of the coated substrates is about 300 HV, which is 4–5 times higher than that of the uncoated substrate. Furthermore, the microhardness of PEO coated AZ31 Mg substrates with Ta_2O_5 nanoparticles is higher than that of pure PEO coatings. In addition, the hardness value increases with increasing nanoparticles into PEO coatings. The improvement in hardness value was probably due to the formation of a layered framework by the uniform and staggered distribution of nanoparticles in the coating, which led to the densification of PEO coating.[18] This result clearly showed that the addition of Ta_2O_5 nanoparticles can enhance the load-bearing tendency of PEO-coated AZ31 Mg substrates.

3.5. Contact angle studies

The effect of Ta_2O_5 nanoparticles on surface wettability of PEO coatings was evaluated by contact angle measurements and the acquired data are shown in Table 2. The contact angle of uncoated AZ31 Mg was found to be 71.6°, whereas that of PEO-coated AZ31 Mg without nanoparticles was found to be 48.2°, which indicated the hydrophobic nature of uncoated and PEO-coated AZ31 Mg. However, PEO-coated AZ31 Mg with Ta_2O_5 nanoparticles showed lower contact angle values compared

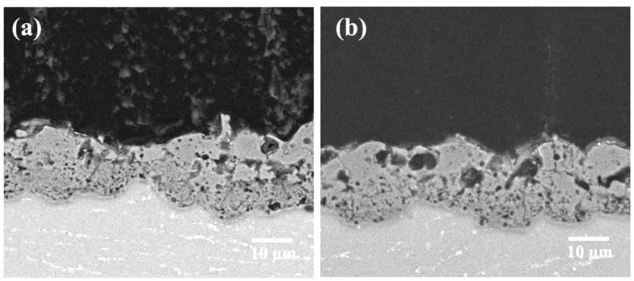

Fig. 4 Cross-sectional SEM images of (a) PEO and (b) Ta10 coatings on AZ31 Mg substrates.

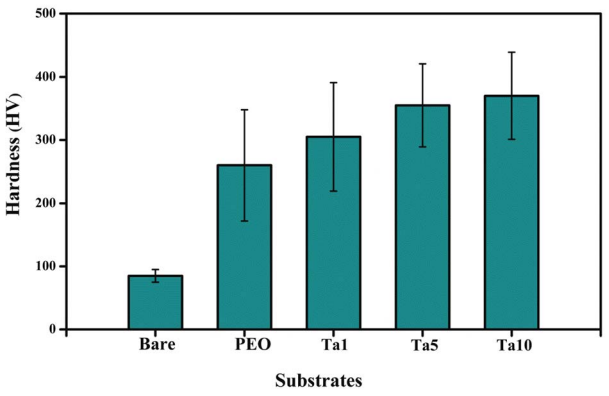

Fig. 5 Microhardness values of PEO coated AZ31 Mg with and without Ta_2O_5 nanoparticles.

Table 2 Contact angle values of PEO coated AZ31 Mg with and without Ta_2O_5 nanoparticles

S. no.	Sample	Contact angles
1	Uncoated	71.6°
2	PEO	48.2°
3	Ta1	24.6°
4	Ta5	14.9°
5	Ta10	12.7°

with pure PEO-coated AZ31 Mg, thus indicating a more hydrophilic surface. It has already been reported that the hydrophilic nature of coatings over implants improves ion exchange behavior from SBF solution, which in turn enhances apatite growth.[19] In addition, it was clearly observed that the contact angle values decreased with increasing Ta_2O_5 nanoparticles into PEO coatings. The results of our study enable us to conclude that the incorporation of Ta_2O_5 into a PEO coating influences its wettability; thus, it is expected to significantly alter its biological functions.

3.6. Tribological studies

3.6.1 CoF and wear rate behavior. Fig. 6a shows the friction coefficient of PEO coatings with and without Ta_2O_5 nanoparticles under 50 mN against an Al_2O_3 ball. Compared with the bare AZ31 Mg substrate, the friction coefficient of PEO coating without and with nano-Ta_2O_5 obviously decreased. For bare substrate, coating initially showed a lower CoF, around 0.2 for 500 cycles, due to the existence of a small amount of oxide layer on the surface. After 500 cycles, the magnitude of CoF increased rapidly, and it showed a value around 0.7 after completing 1800 cycles. For pure PEO coating, CoF value was around 0.25 with consecutive small fluctuation behavior; however, the CoF value of Ta1 coating was found to be about 0.15, which is lower than pure PEO coating. This result evidently indicated that the addition of small amounts of Ta_2O_5 nanoparticles played an important role in reducing the friction behavior of PEO coatings. However, even with a small value of CoF, there was a severe fluctuation with the friction behavior. Ta5 coating showed values almost similar to Ta1, but it was found to exhibit a very stable friction behavior without any fluctuation. Furthermore, the CoF value of Ta10 coating exhibited was about 0.3, and it followed a similar kind of behavior as shown by pure PEO coating with severe fluctuation. The coating wear rates are shown in Fig. 6b. As the Ta_2O_5 content increased from 1 to 10 mg L^{-1}, the wear rate of PEO decreased. The values obtained showed that the coating wear rate of bare substrate was 18.6 μm^3 per (cycle mN), pure PEO was 1.1 μm^3 per (cycle mN), 0.7 μm^3 per (cycle mN) for Ta1, 0.1 μm^3 per (cycle mN) for Ta5 and 1.8 μm^3 per (cycle mN) for Ta10, respectively. In order to elucidate the different behavior of PEO coatings with Ta_2O_5 nanoparticles, surface roughness was measured and the results are shown in Fig. 7(a–d). From the surface profilograph, it could be clearly seen that the surface roughness of the PEO coatings increased with Ta_2O_5 addition because of increase in the number of pores and microcracks as mentioned in SEM analysis. In particular, Ta10 coating exhibited different wear behavior due to its different surface morphology and higher roughness. Furthermore, the coefficient of friction and wear rate would be expected to change with the addition of Ta_2O_5 because nanoparticles affect the formation of transfer film, which is discussed in the following section.

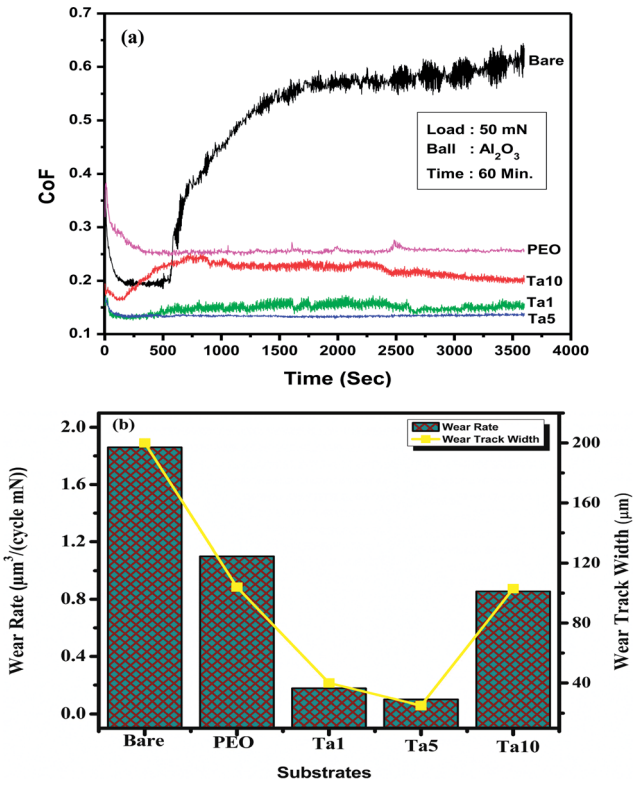

Fig. 6 (a) CoF values of PEO coated AZ31 Mg with and without Ta_2O_5 nanoparticles. (b) Wear rate and wear track width values of PEO coated AZ31 Mg with and without Ta_2O_5 nanoparticles.

3.6.2 Wear track behavior. Fig. 8 displays the SEM image of the wear tracks and corresponding counter surface wear behavior. Fig. 8(a–d) shows SEM micrographs of the wear tracks for pure PEO and Ta1, Ta5, and Ta10 coatings, respectively, in lower magnification. As shown in Fig. 8a, the PEO surface has been partially damaged against Al_2O_3 counter surface, which confirmed its poor anti-wear property. Furthermore, the wear track for this coating is ~104 μm wide, whereas PEO coating with Ta1 coating showed very little damage with wear track width of only ~45 μm. It is clear that Ta_2O_5 nanoparticles play a dominant role in reducing the friction coefficient and wear behavior of PEO coatings. However, Ta5 coating showed excellent wear behavior, with wear track width of only 25 μm, which is evidence of good wear resistance. On the other hand, Ta10 coating exhibited entirely different wear behavior from that of Ta1 and Ta5. Furthermore, Ta10 coating was almost removed from the substrate, which indicates its ploughing behavior. In addition, detailed analyses have been carried out by SEM micrographs of the wear tracks at higher magnification, which are shown in Fig. 8(e–h). In the case of wear track regions in pure PEO coating, many debris were observed along with

parallel grooves produced by the counter surface as shown in Fig. 8e, whereas some dark places were found in the wear track of Ta1 and Ta5, indicating that they are compact and deformed in nature. This is caused by the nanoparticle addition and different surface morphology, which describes the periodic change of CoF.[20] In the case of Ta5, the result showed excellent wear resistance because of the absence of the debris that did not peel off; moreover, they also indicate that only the adhesive wear process was involved. In the case of Ta10, there was complete removal of the debris from the coating, which can be related to parameters such as hardness and morphological behavior.

3.6.3 Transfer film behavior. After the friction test, counter surface morphology of Al_2O_3 was investigated using SEM. Fig. 8(i–l) shows SEM micrographs of the counter surface (Al_2O_3) against pure PEO, Ta1, Ta5 and Ta10, respectively. It is clear from Fig. 8(i) that the Al_2O_3 ball acted against PEO coating. It can also be seen that large amounts of coating were transferred from the wear track to the counter surface, which indicates less wear resistance behavior of the coating. This development of uneven nature of transfer film in contact with PEO coating is due to high friction value and cohesion nature.[21] However, Ta1 and Ta5 coatings showed transfer film behavior that was different from pure PEO coating. In these cases, the nature of the transfer film covered by the ball did not separate the ball as shown in Fig. 8(j and k). High coverage and less film transfer helped in reducing the friction coefficient, which resulted in excellent wear resistance. The transfer film prevents direct contact between the coating pin and the metal counter face, which avoids abrasive action thus results in reduced wear.[22] Particularly, the Ta5 coating with the ball showed a grooving effect due to the excellent wear resistance of the coating. On the other hand, the Ta10 coating showed transfer film behavior that was different from previous coatings.

3.7. Potentiodynamic polarization results

Representative polarization curves of uncoated and PEO coated AZ31 Mg substrate are presented in Fig. 9, and the determined Tafel fitting results of the corrosion potential (E_{corr}) and the corrosion current density (i_{corr}), which are extracted from Tafel

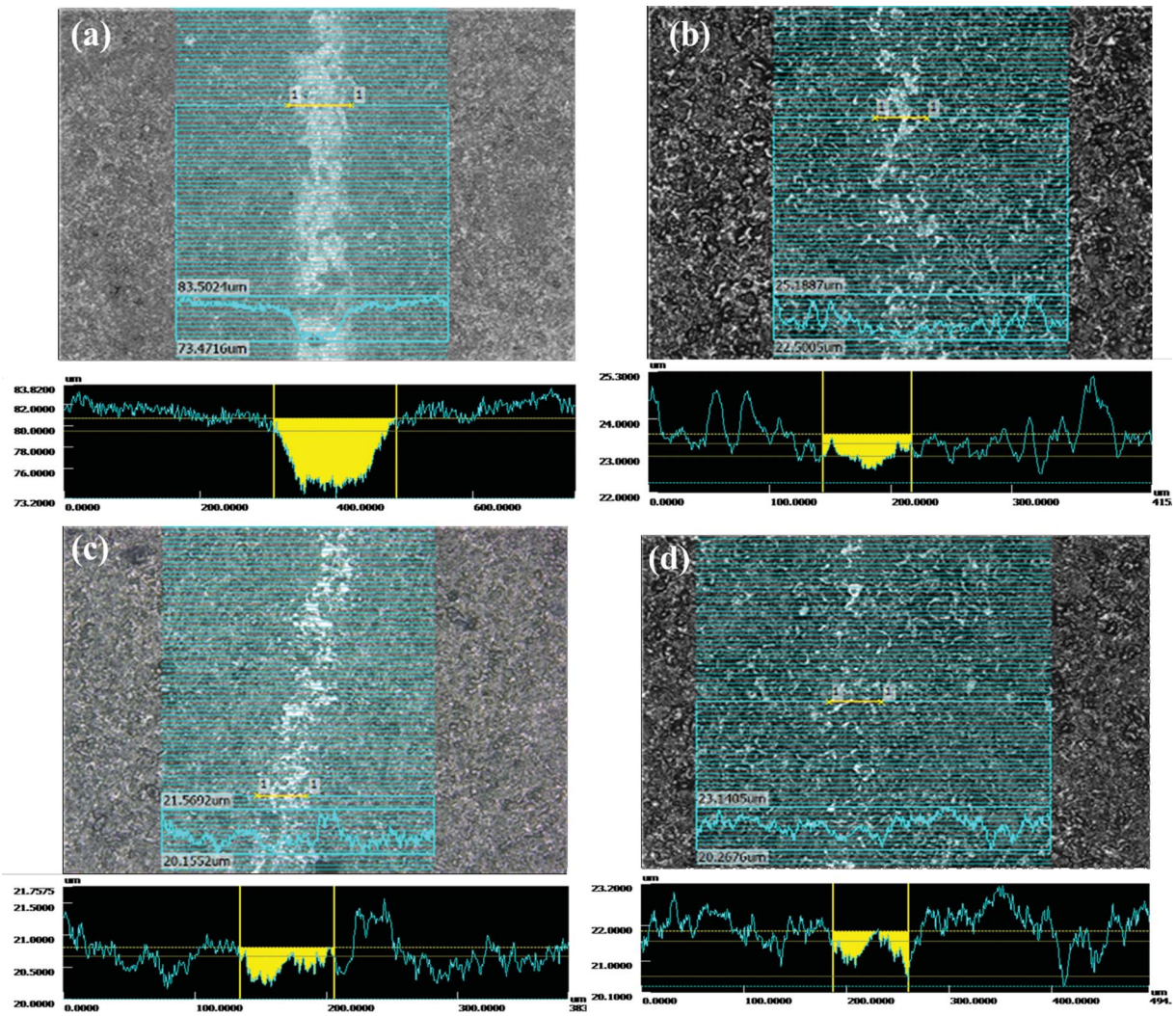

Fig. 7 Surface roughness measurements results of (a) bare (b) PEO (c) Ta5 and (d) Ta10 coatings.

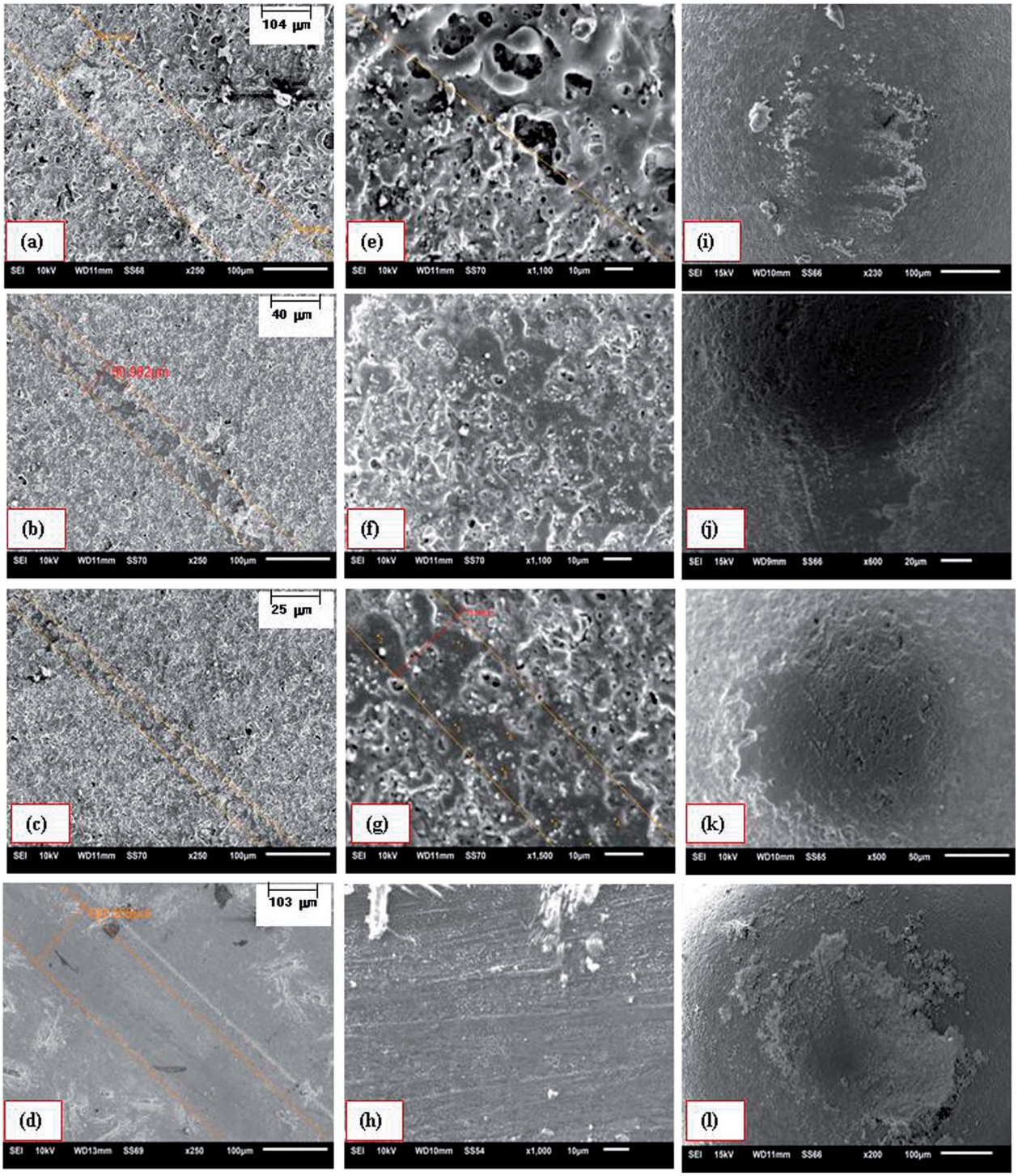

Fig. 8 SEM images of (a) PEO (b) Ta1 (c) Ta5 (d) Ta10 coatings; higher-magnification images of (e) PEO (f) Ta1 (g) Ta5 (h) Ta10 coatings; and SEM images of counter surface against (i) PEO (j) Ta1 (k) Ta5 (l) Ta10 coatings after wear test.

curves are listed in Table 3. Compared with the AZ31 Mg substrate, the corrosion potential (E_{corr}) of PEO coatings was positively shifted by about 250–400 mV and the corrosion current density (i_{corr}) was lowered by 2–3 orders of magnitude as a result of adequate corrosion protection to the Mg alloy in the SBF medium. Moreover, the corrosion current densities of the coated substrates decrease in the order: PEO > Ta1 > Ta5 > Ta10. This indicated that the coating produced from electrolyte with nanoparticles has superior corrosion resistance. It can also be seen that PEO coating with 10 mg L^{-1} of Ta_2O_5 nanoparticles exhibited highest corrosion protection performance among the four coatings. The protection efficiency (PE) of the ceramic coatings was calculated using the following expression,

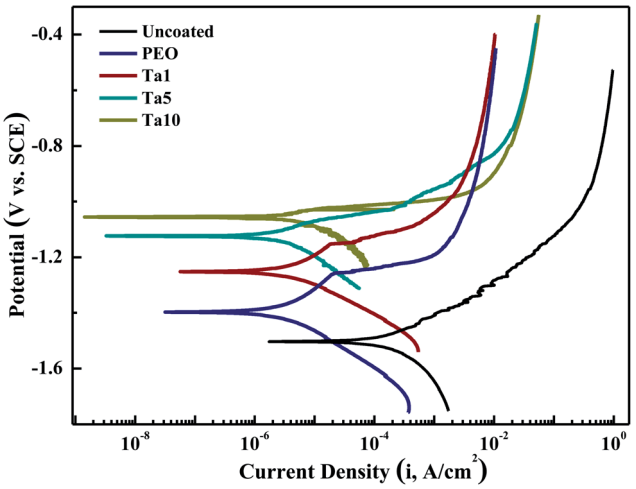

Fig. 9 Tafel curves of PEO coated AZ31 Mg with and without Ta_2O_5 nanoparticles.

$$PE(\%) = \frac{R_{pol}(coated) - R_{pol}(uncoated)}{R_{pol}(coated)} \times 100 \qquad (2)$$

The PEs of PEO ceramic coatings calculated from potentiodynamic polarization data are found to be 94.80%, 96.52%, 98.40% and 98.25% for pure PEO, Ta1, Ta5 and Ta10, respectively. Furthermore, this result indicated that the PEO coatings processed with nanoparticles have superior protection efficiency than pure PEO coatings.

3.8. EIS results

EIS was employed to gain insight into the corrosion protection afforded by the PEO coatings. Fig. 10 represents the Bode plot of uncoated and PEO coated AZ31 Mg substrates. The impedance of the uncoated AZ31 Mg substrate was found to be about 10^3 Ω cm^2, whereas the impedance of PEO coatings was about 10^5 Ω cm^2. The maximum total impedance offered by all these PEO coatings is about two orders of magnitude higher in the low-frequency region, and by at least an order of magnitude higher in the high-frequency region as compared with the uncoated substrate, indicating the improved corrosion performance of coated substrates. Bode phase angle plots for uncoated AZ31 Mg substrate indicated the existence of a single time constant with the maximum phase angle in the low-frequency region, pointing to corrosion activity at the substrate surface. EIS spectra obtained on the PEO-coated substrates are characterized by the presence of two time constants: one in the high-frequency region, attributed to the presence of PEO layer, and another one in the lower frequencies, representing the charge transfer reaction accompanied by oxidation of the substrate. Based on the proposed equivalent circuit model in Fig. S5,† the EIS spectra were analyzed and the curve fitting was performed for all the substrates, which showed an excellent agreement between the experiments and the fitting. Considering the impedance values from the figure, the protective performance offered by these coatings can be ranked as PEO > Ta1 > Ta5 > Ta10. Based on the above results, it was concluded that the PEO coatings with Ta_2O_5 nanoparticles are most suitable to protect Mg alloys against corrosive environments.

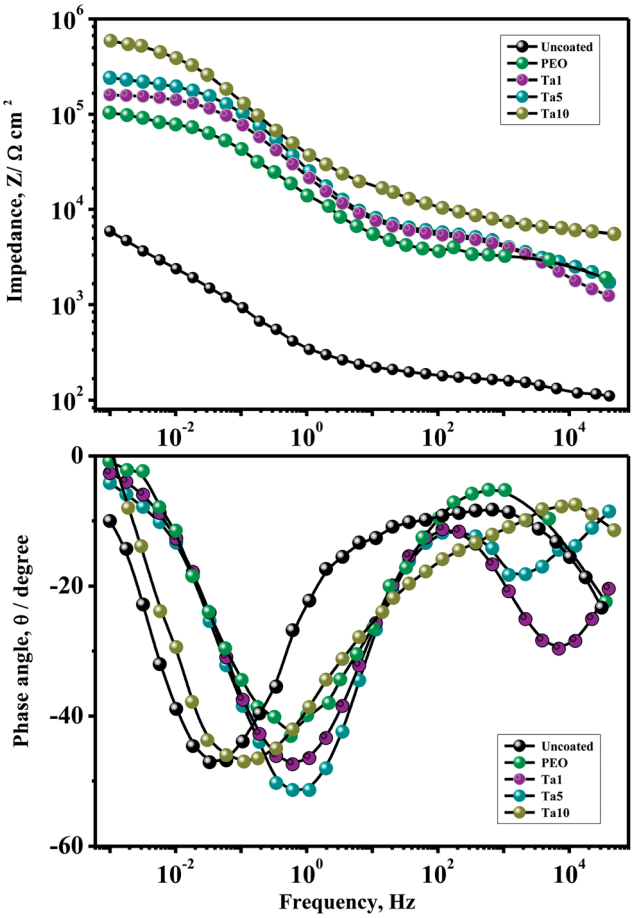

Fig. 10 Bode plots of PEO coated AZ31 Mg with and without Ta_2O_5 nanoparticles.

Table 3 Tafel parameters for PEO coated AZ31 Mg with and without Ta_2O_5 nanoparticles

Sample	E_{corr} mV (SCE)	i_{corr} μAcm^{-2}	β_a mV dec^{-1}	β_c mV dec^{-1}	Protection efficiencies (%)
Uncoated	−1.4973	25.811	65	54	—
Pure PEO	−1.3970	0.6158	53	78	94.80
Ta1	−1.2544	0.1430	72	67	96.52
Ta5	−1.1211	0.0721	58	69	98.40
Ta10	−1.0512	0.0712	72	83	98.25

3.9. *In vitro* biocompatibility test

In order to evaluate the biocompatibility behavior of uncoated and coated AZ31 Mg substrates, MG-63 cell culture studies were performed, and equal numbers of MG-63 cells were cultured on different sterile specimens and incubated for 3 and 7 days. Live cells are stained with calcein AM fluorescent dye, which is retained within live cells and emits green fluorescence. In general, corrosion of the magnesium alloy leads to the formation of magnesium hydroxide; thus, the pH rises above 8. The increase in pH together with the detachment of the corrosion layer makes cell adhesion difficult; hence, lowering the corrosion rate and surface modification by bioactive coatings is expected to improve the cell behavior. Fig. 11a shows the cell culture response of the uncoated and coated AZ31 Mg substrates for the period of 3 and 7 days, respectively. From the results, it can be clearly seen that cell growth was higher in coated substrates with Ta_2O_5 nanoparticles compared to pure PEO and uncoated AZ31 Mg substrates. The growth of the cells increased proportionally with the increased concentration of Ta_2O_5 on AZ31 Mg substrates. In particular, significantly higher densities of MG-63 were obtained on AZ31 Mg substrate coated with Ta10 when compared with AZ31 Mg substrate coated with

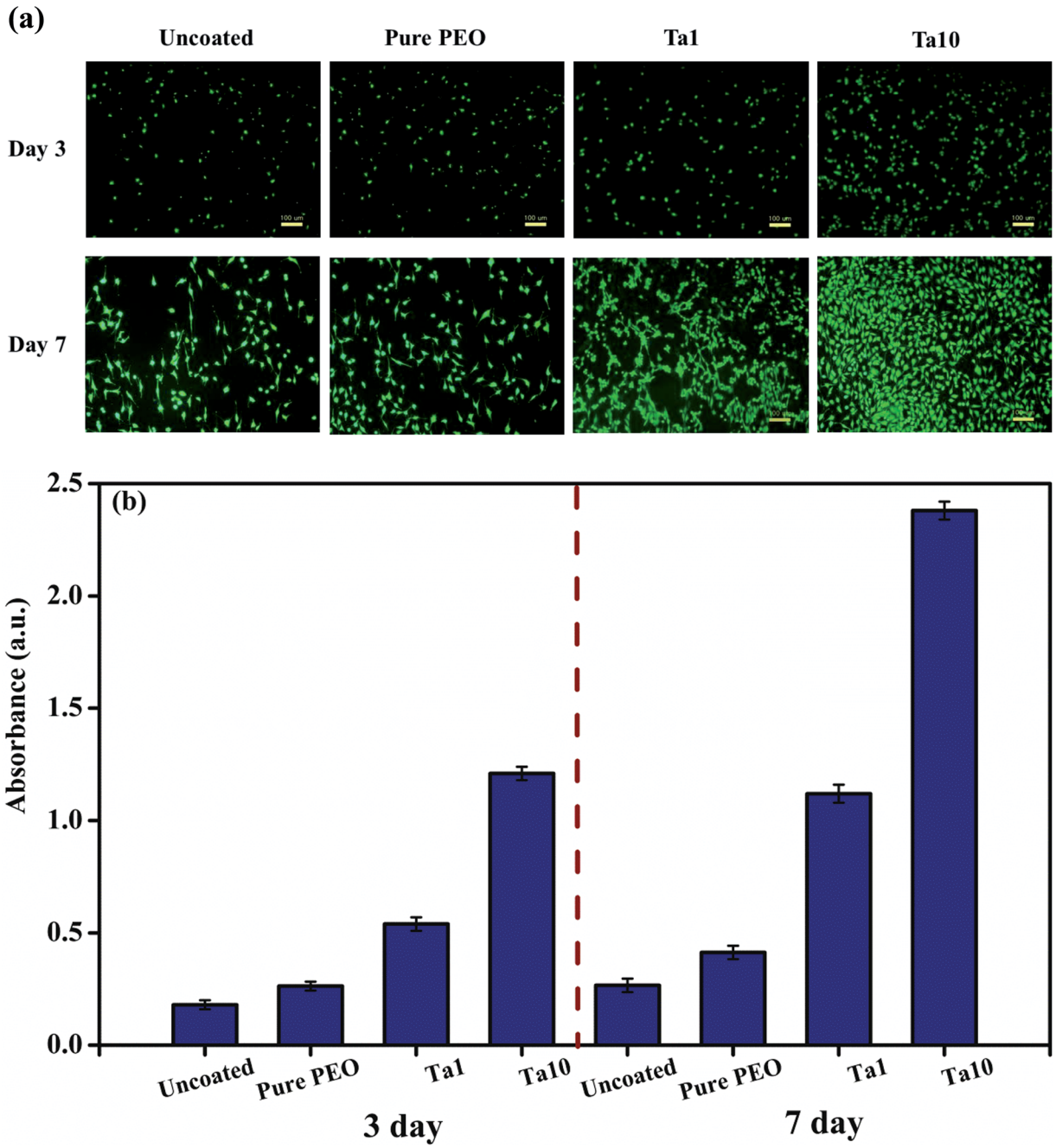

Fig. 11 *In vitro* cell culture responses from uncoated and coated AZ31 Mg substrates.

Table 4 Interaction energy of Mg–Ta_2O_5 complex

Systems	E_{Mg}	$E_{Ta_2O_5}$	$E_{Mg-Ta_2O_5}$	E_{ads}
Energies (Atomic Units)	−8.8199	−491.98	−492.87	−1.709

Table 5 Some adsorption parameters (kcal mol^{-1}) of $Mg_3(PO_4)_2$ interaction on top of MgO (001) surface calculated from adsorption locator module

Total energy	Adsorption energy	Rigid adsorption deformation energy
-3.39×10^3	−182.40	−186.303

pure PEO and Ta1. Healthy morphology of MG-63 cells with polygonal shape and filopodial extensions were observed on AZ31 Mg substrate coated with Ta10. Our results are consistent with the previous studies, reporting that nanostructuring significantly alters the proliferation of fibroblast and osteoblast cells in comparison to flat substrates.[23]

In order to corroborate the above results, we have also carried out the cell proliferation assay on MG-63 cells cultured on bioimplants using a CCK-8 kit. Equal numbers of cells were seeded on AZ31 Mg substrates coated with different concentrations of Ta_2O_5 substrates and allowed to grow for 3 and 7 days. As a result, high cell proliferation was observed in AZ31 Mg substrate coated with Ta10 when compared with the AZ31 Mg substrate coated with pure PEO or Ta1. The cell growth increased significantly as the concentration of Ta_2O_5 on AZ31 Mg substrates was increased (Fig. 11b). The percentage of cell growth obtained from coated substrates with Ta_2O_5 nanoparticles was higher when compared with pure PEO and uncoated substrates. In addition, the rate of cell proliferation on coated substrates with 10 mg of Ta_2O_5 was significantly higher, about 3 times higher than the growth rate on coated substrates with 1 mg of Ta_2O_5. In good agreement with our previous cell staining results, we found that AZ31 Mg substrate coated with Ta_2O_5 substrates allow high cell adhesion and cell growth behavior of MG-63 cells. Our results suggest that the biocompatibility behavior of MG-63 was best for 10 mg Ta_2O_5-doped PEO-coated AZ31 Mg substrates.

3.10. Quantum chemical studies

3.10.1 Quantum chemical insights into the reactivity of Mg alloy with Ta_2O_5. In order to verify the experimental results, quantum chemical theoretical modeling was employed to describe the role of Ta_2O_5 nanoparticles on PEO coatings. The reactions involving the PEO coating of Mg alloy using phosphate electrolyte are known to proceed with the following mechanisms:

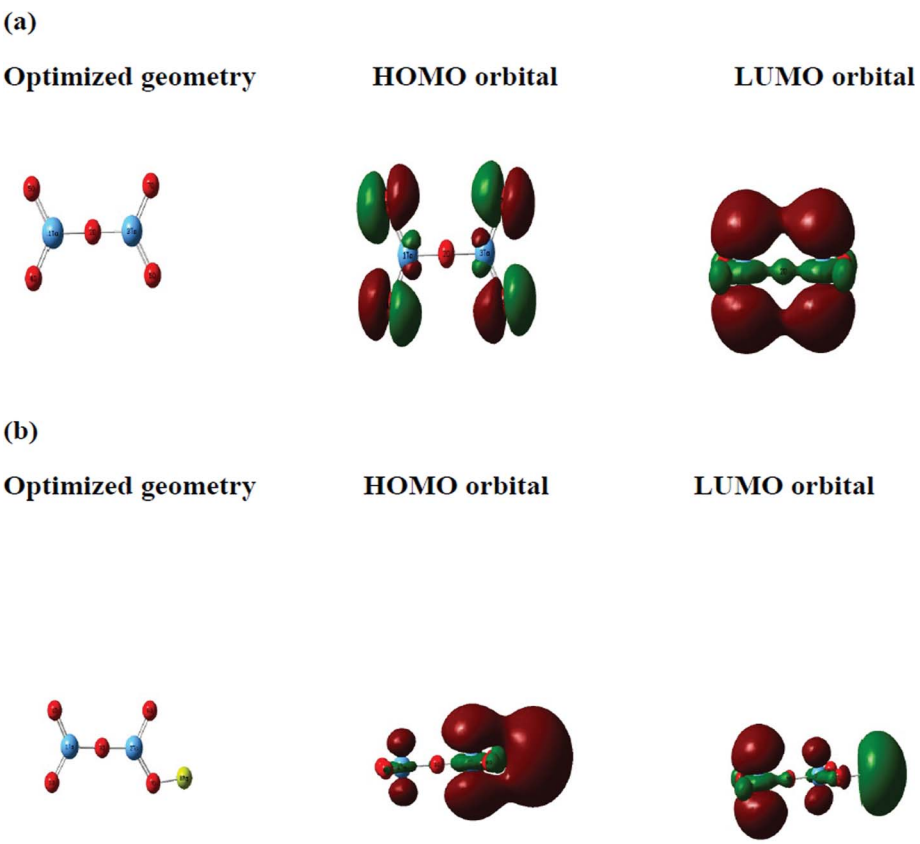

Fig. 12 The optimized structure, HOMO orbital and the LUMO orbital of (a) Ta_2O_5 and (b) the stable Mg–Ta_2O_5 complex.

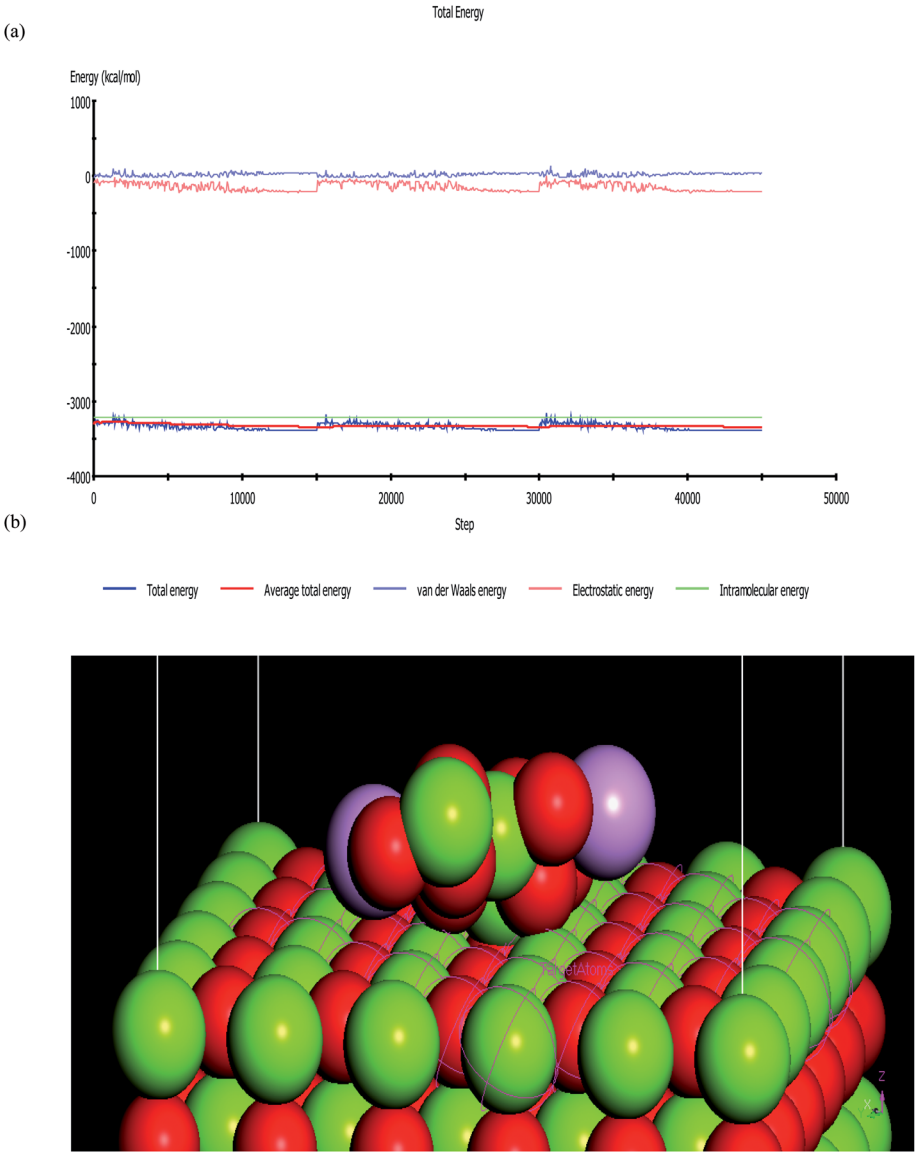

Fig. 13 (a) Equilibrium adsorption energy curves of $Mg_3(PO_4)_2$ interaction on top of MgO surface. (b) The most: stable equilibrium adsorption configuration of $Mg_3(PO_4)_2$ interaction on top of MgO (001) surface. (Colour interpretations: red = oxygen; green = Mg and purple = phosphorus atoms).

Anodic dissolution:

$$Mg \rightarrow Mg^{2+} + 2e^{-} \quad (3)$$

Oxygen-evolution:

$$4OH^{-} \rightarrow 2H_2O + O_2 + 4e^{-} \quad (4)$$

Oxide–electrolyte interface:

$$Mg^{2+} + 2OH^{-} \rightarrow Mg(OH)_2 \quad (5)$$

$$Mg(OH)_2 \rightarrow MgO + H_2O \quad (6)$$

The cation (Mg^{2+}) released from the AZ31 Mg alloy in eqn (3) combines with the anion (PO_4^{3-}) in the electrolyte (Na_3PO_4) to form:

$$3Mg^{2+} + 2PO_4^{3-} \rightarrow Mg_3(PO_4)_2 \quad (7)$$

MgO is formed from dehydration of the unstable $Mg(OH)_2$ at the high temperature resulting from the plasma discharge.

The experimental results obtained from this study show that the addition of Ta_2O_5 nanoparticles to PEO ceramic coatings has a beneficial role in enhancing their tribological and corrosion protection performance. We apply the methodology of quantum chemical calculations to provide addition information on the mechanism of interaction of Ta_2O_5 with Mg at the atomic level. Quantum chemical calculations have been widely

used to study reaction mechanisms; moreover, they have also proved to be a very important tool for studying corrosion inhibition mechanisms. In recent times, density functional theory (DFT) has become an attractive theoretical method because it gives exact basic vital parameters for materials at low cost. DFT has been employed as a powerful technique to probe the adsorbate/substrate interaction and to analyze experimental data. Becke's three-parameter functional (B3), which includes a mixture of HF with DFT exchange terms associated with the gradient-corrected correlation functional of Lee, Yang and Parr (LYP), was used in this investigation to carry out quantum calculations. Full geometry optimization together with vibrational analysis of the optimized structures of Mg and Ta_2O_5 were carried out at the B3LYP/LANL2DZ level of theory using the Gaussian 03 program package.[24]

The geometry of the Ta_2O_5–magnesium (single Mg atom) system was optimized *via* the B3LYP/LANL2DZ method. The modeling of the interaction between a single metal atom and a molecule or compound is well established in quantum chemical calculation and is widely reported.[25,26] The value of the interaction energy between Mg and Ta_2O_5 was computed in order to understand the energetics and the stability of the formed Mg–Ta_2O_5 complex. The calculations showed that the interaction energy (E_{ads}) of Ta_2O_5 with Mg obtained was negative, which indicates that the adsorption occurs spontaneously and a stable Mg–Ta_2O_5 complex is formed (Table 4). The result confirms the enhanced activity and stability of PEO coating for the protection of AZ31 Mg alloy in the presence of Ta_2O_5. The optimized structure, HOMO orbital and the LUMO orbital of Ta_2O_5 and the stable Mg–Ta_2O_5 complex are shown in Fig 12(a) and (b), respectively. It is clear from Fig. 12a that the HOMO level of Ta_2O_5 is mainly localized around the four oxygen atoms, which could be considered as electron donor centers, whereas the LUMO is localized on the entire system (that is, both O and Ta atoms). These centers have the ability to accept electrons from a donor atom (Mg). Moreover, it can be seen from Fig. 12b that the most stable Mg–Ta_2O_5 complex is formed due to the interaction of the Ta_2O_5 with Mg using the electron lone pairs on its oxygen atoms. The HOMO and LUMO orbitals also spread around the four oxygen atoms on the two sides of Ta_2O_5, and these sites are the major reactive center for interaction with Mg. The Ta atom is also involved in the bond formation as shown in the HOMO and LUMO orbitals of the Mg–Ta_2O_5 complex (Table 5).

The interaction energy between the Ta_2O_5 and Mg was calculated using the following equation:

$$E_{ads} = E_{Mg\text{–}Ta_2O_5} - (E_{Ta_2O_5} - E_{Mg}) \quad (8)$$

where E_{Mg} is the total energy of the Mg atom, and $E_{Ta_2O_5}$ is the total energy of Ta_2O_5. When adsorption occurs between the compound and Mg, the energy of the new system is expressed as $E_{Mg\text{–}Ta_2O_5}$.

3.10.2 Molecular dynamics simulations of $Mg_3(PO_4)_2$ on MgO surface. It has been determined from the experimental investigation that $Mg_3(PO_4)_2$ is formed on top of a thin film of MgO. Therefore, molecular dynamics simulation was further employed to determine the stability of $Mg_3(PO_4)_2$ formed on top of a MgO surface. The simulation was carried out using Material Studio Software version 6.0 from Accelrys Inc. (USA).[24] A stable MgO (001) was sketched and optimized together with Ta_2O_5 using the COMPASS force field implemented in the Forcite module. The adsorption locator module was used in the simulation of the adsorption of $Mg_3(PO_4)_2$ on top of the MgO surface. The MgO (001) was modeled with a simulation box of 14.88 × 14.88 × 30.52 Å with a fractional thickness of 3.0 Å. A supercell of dimension 5 × 5 was further constructed to ensure enough surface area for the interaction. The COMPASS (Condensed Phase Optimized Molecular Potentials for Atomistic Simulation Studies) force field, which we employ to optimize the structures of all components of the designated system, represents a technological breakthrough in force field method. It is the first *ab initio* force field that enables accurate and simultaneous prediction of chemical and condensed-phase properties for a broad range of chemical systems.[25,27,28] Fig. 13(a) depicts the equilibrium adsorption energy plots during the adsorption of $Mg_3(PO_4)_2$ on top of the MgO surface. It is clear from the figure that the system reached equilibrium, *i.e.* no marked fluctuation in the curves. Moreover, Fig. 13(b) shows the lowest and the most stable equilibrium adsorption energy of $Mg_3(PO_4)_2$ on top of the MgO surface. It is evident that the interaction of $Mg_3(PO_4)_2$ with MgO was mainly through the oxygen atoms of the phosphate groups. The adsorption energy is presented in Table 5. It is clear that a large negative adsorption energy was obtained. This can be attributed to strong and stable adsorption of $Mg_3(PO_4)_2$ on top of the MgO surface. Similar results have been documented by other researchers.[29,30] This conclusion is in agreement with the experimental results; hence, based on the above results, there was a stable PEO coating and Ta_2O_5 further improved corrosion performance without compromising the biological and tribological performance of coated AZ31 Mg substrates.

4. Conclusions

PEO ceramic coatings with Ta_2O_5 nanoparticles have been successfully fabricated on AZ31 Mg substrates from phosphate electrolytes. XRD showed that the processed coating comprised mainly MgO in the inner layer and $Mg_3(PO_4)_2$ and Ta_2O_5 nanoparticles on the outer layer of the coating in different quantities depending on the mode of processing. Surface characterization results clearly revealed that the PEO coatings with Ta_2O_5 nanoparticles were thicker and more uniform with no cracks and micropores compared to others. Potentiodynamic polarization and EIS results confirmed the enhanced corrosion performance of PEO ceramic coatings with the addition of Ta_2O_5 nanoparticles due to their dense and more compact layer with the better chemical stability of the $Mg_3(PO_4)_2$ and Ta_2O_5 nanoparticles. The wear resistance of PEO coatings increased for Ta_2O_5 nanoparticles having concentration of 1 and 5 mg L^{-1}, but decreased for those having concentration of 10 mg L^{-1}. Furthermore, MG-63 *in vitro* cell culture studies revealed that the coated AZ31 Mg substrates with Ta_2O_5 nanoparticles facilitate high cell adhesion behavior

of MG-63 cells compared with that of pure PEO and uncoated substrates. Quantum chemical calculations together with molecular dynamics simulation were successfully used to verify the experimental results. Based on the above results, it can be concluded that the addition of Ta_2O_5 nanoparticles to PEO ceramic coatings has a beneficial role in enhancing their tribological and corrosion protection performance without losing the biocompatibility of implants.

Acknowledgements

The authors gratefully acknowledge King Fahd University of Petroleum and Minerals (KFUPM) for providing the facilities for this research. This work was partially supported by the National Research Foundation of Korea (NRF) grant funded by the Korea government (MSIP) (no. 2010–0018289).

References

1 H. Hornberger, S. Virtanen and A. R. Boccaccini, *Acta Biomater.*, 2012, **8**, 2442–2455.
2 J. H. Jo, J. Y. Hong, K. S. Shin, H. E. Kim and Y. H. Koh, *J. Biomater. Appl.*, 2012, **27**, 469–476.
3 M. H. Lee, I. Y. Bae, K. J. Kim, K. M. Moon and I. Oki, *Surf. Coat. Technol.*, 2003, **169**, 670–674.
4 Z. P. Yao, Y. J. Xu, Y. F. Liu, D. L. Wang, Z. H. Jiang and F. P. Wang, *J. Alloys Compd.*, 2011, **509**, 8469–8474.
5 H. S. Ryu, S. J. Mun, T. S. Lim, H. C. Kim, K. S. Shin and S. H. Hong, *J. Electrochem. Soc.*, 2011, **158**, C266–C273.
6 X. H. Wu, P. B. Su, Z. H. Jiang and S. Meng, *ACS Appl. Mater. Interfaces*, 2010, **2**, 808–812.
7 A. L. Yerokhin, X. Nie, A. Leyland, A. Matthews and S. J. Dowey, *Surf. Coat. Technol.*, 1999, **122**, 73–93.
8 F. Liu, D. Y. Shan, Y. W. Song and E. H. Han, *Trans. Nonferrous Met. Soc. China*, 2011, **21**, 943–948.
9 T. S. Lim, H. S. Ryu and S. H. Hong, *Corros. Sci.*, 2012, **62**, 104–111.
10 Y. Han and J. F. Song, *J. Am. Ceram. Soc.*, 2009, **92**, 1813–1816.
11 C. Y. Zhao, K. L. Liang, J. Tan, Z. Xiang, H. S. Fan and X. D. Zhang, *Biomed. Mater.*, 2013, 8.
12 N. Donkov, A. Zykova, V. Safonov, R. Rogowska, J. Smolik and V. Luk'yanchenko, *Problems of Atomic Science and Technology*, 2011, 131–133.
13 P. B. Srinivasan, J. Liang, C. Blawert, M. Stormer and W. Dietzel, *Appl. Surf. Sci.*, 2010, **256**, 4017–4022.
14 H. F. Guo and M. Z. An, *Appl. Surf. Sci.*, 2005, **246**, 229–238.
15 K. M. Lee, K. R. Shin, S. Namgung, B. Yoo and D. H. Shin, *Surf. Coat. Technol.*, 2011, **205**, 3779–3784.
16 A. Ghasemi, V. S. Raja, C. Blawert, W. Dietzel and K. U. Kainer, *Surf. Coat. Technol.*, 2008, **202**, 3513–3518.
17 X. J. Li, X. Y. Liu and B. L. Luan, *Appl. Surf. Sci.*, 2011, **257**, 9135–9141.
18 Y. Kim, D. Kim, H. Park, U. Chung and W. Chung, in *11th International Conference on the Mechanical Behavior of Materials*, ed. M. Guagliano and L. Vergani, 2011, vol. 10.
19 A. M. Kumar and N. Rajendran, *Surf. Coat. Technol.*, 2012, **213**, 155–166.
20 P. B. Srinivasan, C. Blawert and W. Dietzel, *Wear*, 2009, **266**, 1241–1247.
21 A. Amanov, S. Sasaki, D. E. Kim, O. V. Penkov and Y. S. Pyun, *Tribol. Int.*, 2013, **64**, 24–32.
22 E. Thangavel, S. Ramasundaram, S. Pitchaimuthu, S. W. Hong, S. Y. Lee, S. S. Yoo, D. E. Kim, E. Ito and Y. S. Karig, *Compos. Sci. Tech.*, 2014, **90**, 187–192.
23 A. Madhankumar, S. Ramakrishna, P. Sudhagar, H. Kim, Y. Kang, I. B. Obot and Z. Gasem, *J. Mater. Sci.*, 2014, **49**, 4067–4080.
24 M. J. Frisch, G. W. Trucks and H. B. Schlegelet, *Gaussian 03W*, Gaussian Inc., Wallingford CT, 2004.
25 M. S. Masoud, M. K. Awad, A. E. Ali and M. M. T. El-Tahawy, *J. Mol. Struct.*, 2014, **1062**, 51–59.
26 N. O. Obi-Egbedi, I. B. Obot and M. I. El-Khaiary, *J. Mol. Struct.*, 2011, **1002**, 86–96.
27 Materials Studio, *Revision 6.0*, Accelrys Inc., San Diego, USA, 2011.
28 M. M. Kabanda, I. B. Obot and E. E. Ebenso, *Int. J. Electrochem. Sci.*, 2013, **8**, 10839–10850.
29 I. B. Obot, E. E. Ebenso and M. M. Kabanda, *Int. J. Chem. Environ. Eng.*, 2013, **1**, 431–439.
30 I. B. Obot, N. O. Obi-Egbedi, E. E. Ebenso, A. S. Afolabi and E. E. Oguzie, *Res. Chem. Intermed.*, 2013, **39**, 1927–1948.